Stress-mediated solution deposition method to stabilize ferroelectric $BiFe_{1-x}Cr_xO_3$ perovskite thin films with narrow bandgaps

*Ricardo Jiménez[1], Jesús Ricote[1], Iñigo Bretos[1], Rafael J.Jiménez Riobóo[1], Federico Mompean[1], Ana Ruiz[1], Haibing Xie,[2] Mónica Lira-Cantú[2] and M. Lourdes .Calzada[1]**

[1] Instituto de Ciencia de Materiales de Madrid (ICMM). Consejo Superior de Investigaciones Científicas (CSIC). C/ Sor Juana Inés de la Cruz 3, Cantoblanco. Madrid 28049. Spain.

[2] Catalan Institute of Nanoscience and Nanotechnology (ICN2), CSIC and the Barcelona Institute of Science and Technology (BIST). Building ICN2, Campus UAB E-08193, Bellaterra, Barcelona, Spain.

Keywords: Thin film, perovskite, chemical solution deposition, ferroelectricity, bismuth ferrite, bandgap.

Abstract. Ferroelectric oxides with low bandgaps are mainly based on the $BiFeO_3$ perovskite upon the partial substitution of iron with different cations. However, the structural stability of many of these perovskites is only possible by their processing at high pressures (HP, >1GPa) and high temperatures (HT, >700ºC). Preparation methods under these severe conditions are accessible to powders and bulk ceramics. However, transferring these conditions to the fabrication of thin films is a challenge, thus limiting their use in applications. Here, a chemical solution deposition method is devised, which overcomes many of these restrictions. It is based on the application of an external compressive-stress to the film sample during the thermal treatment required for the film crystallization, promoting the formation and stabilization of these HP perovskites. We demonstrate the concept on $BiFe_{1-x}Cr_xO_3$ (BFCO) thin films deposited on $SrTiO_3$ (STO) substrates and with large chromium contents. The

resulting BFCO perovskite films show narrow bandgaps (Eg~2.57 eV) and an excellent ferroelectric response (remnant polarization, P_R~ 40 μC cm^{-2}). The polarized thin films under illumination present a large out-put power of ~6.4 μW cm^{-2}, demonstrating their potential for using in self-powered multifunctional devices. This stress-mediated solution deposition method can be extended to other perovskite films which are unviable under conventional deposition methods.

1. Introduction

Solar-based technologies are promising energy source capable to generate macroscale power (>W level) for industrial and domestic use.[1] However, at the microscale (from nW to mW), the idea of energy harvesting becomes important. In these microsystems, energy from light is harvested and converted into usable micropower electricity to supply wireless sensor networks (WSNs) formed by self-powered smart-devices.[2, 3] Indeed, the exploitation of the photovoltaic effect in multifunctional materials like ferroelectrics (an example of multifunctionallity) shows huge opportunities in this field.[4, 5] Photovoltaic ferroelectric devices could autonomously power themselves with micropower electricity without the need of maintenance, and at the same time, could operate with multiple functions (e.g., memories, sensors or actuators). Therefore, ferroelectric oxides are foreseen as ideal candidates for self-powered devices.[2, 3, 6-11]

The bismuth ferrite ($BiFeO_3$) is an intrinsic multiferroic compound with a rhombohedral distorted perovskite structure. It shows ferroelectric, ferroelastic and antiferromagnetic properties at room temperature.[12] During the last decade, this lead-free perovskite family has drawn enormous interest in many fields, including solar photovoltaics, due to its narrow bandgap (E_g ~ 2.8 eV), non-toxicity and its chemical and structural stability.[6, 13] Solid solutions of $BiFeO_3$ and $BiMO_3$ perovskites with M = Cr, Mn, Co or Ni, show high ferroelectric polarization and lower bandgap in relation to the pure $BiFeO_3$.[14-18] However,

the preparation of these $BiMO_3$ perovskites have only been attained as powders or as bulk ceramics applying unconventional synthesis conditions like high temperature (HT) and high pressure (HP).[17, 19, 20] Recently, the application of these compounds as solar absorbers has been demonstrated for solid solutions of $BiFeO_3$ and $BiCrO_3$ (also formulated as $BiFe_{1-x}Cr_xO_3$, herein BFCO), where large amounts of chromium are introduced in the double perovskite (i.e., $BiFe_{0.5}Cr_{0.5}O_3$).[21]. Both $BiFeO_3$ and $BiCrO_3$ are insulators with energy bandgaps of ~2.8 eV and ~1.4 eV, and with maximum theoretically calculated values of spontaneous polarization, P_S, of ~95 μC cm^{-2} and ~67 μC cm^{-2},[14, 22] respectively. The $BiFe_{0.5}Cr_{0.5}O_3$ perovskite has been stabilized in thin films on $SrTiO_3$ (STO) substrates by pulsed laser deposition (PLD), applying extremely thorough PLD parameters. The use of the STO substrate is preferred due to the compressive stress that imposes to the BFCO layer, which facilitates an epitaxial growth of the thin film.[21, 23, 24] Notably, the application of an epitaxial strain during the thin film crystallization forces the incorporation of chromium into the perovskite structure stabilizing the metastable BFCO perovskite phase. In addition, it also seems to affect the amount of Fe^{2+}/Cr^{4+} cationic ordering obtained in the perovskite film, which has been related to the origin of the narrow bandgap.[21] As a result, complete solar cells with a power conversion efficiency of ~3.3 % have been obtained, [21] which is the highest efficiency obtained for a photovoltaic device applying a ferroelectric oxide material as the only absorber. Despite the possibility to fabricate and stabilize narrow-bandgap metastable ferroelectric perovskites as thin films, the need for severe processing conditions during thin film formation is a drawback for the deployment of applications where scalable and mass-production technology is required [21, 25-28]

In this work, we devise for the first time, a low-cost, solution deposition method to fabricate thin films of $BiFe_{1-x}Cr_xO_3$ (BFCO) metastable perovskites. The resulting perovskite thin films show narrow bandgap (Eg~2.57 eV) and excellent ferroelectric properties (P_R~ 40 μC cm^{-2}).

The method is based on a modification of the chemical solution deposition (CSD) technique, where a large external stress applied to the solution-deposited layer is maintained through the crystallization of the film during annealing. The extreme pressure conditions applied allow the formation and stabilization of the BFCO perovskite phase in thin film form at low temperatures, ≤ 600ºC. This synthesis strategy can be extended to the fabrication of thin films of many other complex ferroelectric oxides which are difficult to synthesize at ambient pressure. Our synthesis method opens the door to the application of the novel functional properties of these ferroelectric perovskite thin films in the upcoming high-performance devices demanded by society.

2. Experimental procedure

2.1. $BiFe_{1-x}Cr_xO_3$ precursor solutions

Synthesis of the Bi(III) –, Fe(III) – and Cr(III) – precursor solutions was carried out according with a method published elsewhere.[29, 30] Aliquots of these solutions were mixed and diluted in dried ethanol (CH_3-CH_2-OH) to obtain $BiFe_{1-x}Cr_xO_3$ (BFCO) precursors with an equivalent concentration of 0.1 mol/L. No bismuth excess was used. Solutions with different Cr(III) contents were prepared: 0 mol% Cr ($BiFeO_3$, BFO), 3.125 mol% Cr (3.125-BFCO), 6.25 mol% Cr (6.25-BFCO), 12.5 mol% Cr (12.5-BFCO), 25 mol% Cr (25-BFCO) and 50 mol% Cr (50-BFCO).

2.2. Deposition and stabilization of $BiFe_{1-x}Cr_xO_3$ thin films

The solutions were spin coated at 2000 rpm for 45 s on Pt-coated (100) silicon (Pt/Si), (100) $SrTiO_3$ (STO) and $La_{0.7}Sr_{0.3}MnO_3$ coated (100) $SrTiO_3$ (LSMO/STO) substrates. The wet layers were heated at 150 ºC for 5 minutes on a hot-plate, pre-annealed in oven in air atmosphere at a temperature of 250 ºC for 5 min and crystallized by Rapid Thermal Processing (RTP) under ambient pressure at 500 ºC or 600 ºC (the latter for films with a chromium content over 25 mol%) for 10 minutes in argon atmosphere and with a heating rate

of 30 ºC/s. This process was repeated to increase the film thickness.[31] Crystalline films with thickness between 50 nm and 200 nm were prepared. Some of the BFCO films with high chromium contents were subject to a controlled compressive deformation of ~4‰ during the thermal treatment of crystallization, using the home-made stress sample holder shown in Figure 1. The thermal expansion of this sample holder at the crystallization temperature (500ºC-600°C) is negligible. The BFCO films on the STO substrates are held by quartz bars with a low thermal expansion coefficient (~0.5 10^{-6} $°C^{-1}$). These quartz bars are on alumina bars (thermal expansion coefficient of α-alumina ~10.3 10^{-6} $°C^{-1}$), which are supported on a steel holder, also with a low thermal expansion coefficient (7.2 10^{-6} $ºC^{-1}$) (see Figures 1(d) and 1(e)). This design of the holder assures that the force applied during thermal treatment is only used in producing the deformation of the film sample.

2.3. X-ray diffraction analysis

Crystal phases developed in the films were monitored by X-ray diffraction (XRD) using a Bruker powder diffractometer D8 with a Cu anode (λ=1.5418Å) and with a Bragg-Brentano geometry. 2θ scans were recorded between 20º and 80º. Reciprocal space maps (rsm) of the films on STO were acquired around the symmetric (002) and asymmetric (-103) reflections of the $SrTiO_3$, using a high resolution X-ray diffraction Bruker AXS D8 DISCOVER 4-axis diffractometer with a Cu anode and a LynxEye detector. The data recorded were analyzed with the LEPTOS software.

2.4. Optical characterization

Optical characterization was carried out in a spectroscopic ellipsometer SOPRA-GES5E for films on Pt/Si and STO substrates. Tan(Ψ) and Cos(Δ) data were collected at room temperature as a function of the incident light wavelength and using an incident angle of 80º. Experimental data were analyzed with the Winelli II software, considering a heterostructure formed either by a Pt substrate or by a STO substrate, the perovskite film and, if necessary, a

roughness layer on top of the structure. The roughness of the thin film layer was modeled with a Bruggeman effective medium model that considers at the surface of the film a mixture of the perovskite layer and voids. Porosity in the bulk film was not taken into account in these calculations. A Tauc-Lorenz numerical model was used to describe the optical properties of the layered film as proposed by Kumar et al.[32] The layer structure shown in Fiigure S1 was considered in these calculations.[33]

2.5. Field Emission Gun Scanning Electron Microscopy and Energy dispersive X-ray elemental analysis

Cross-sections and plan-view images of the films were obtained by Field Emission Gun Scanning Electron Microscopy (FEGSEM) in a Nova NANOSEM 230 equipment. Energy dispersive X-ray (EDX) elemental mapping of the surfaces of the films was also carried out in this microscope, making the analysis of the Cr-K, Fe-L and Bi-M emissions.

2.6. Piezoresponse Force Microscopy characterization

Topographies of the surfaces of the BFO and BFCO films on STO were obtained by Scanning Force Microscopy, using a commercial microscope (Nanotec® Electrónica controlled by WSxM® software). The local electromechanical characteristics of the films were studied by means of Piezoresponse Force Microscopy (PFM), applying an external AC voltage with amplitudes up to 1.5 V and a frequency of 50 kHz between the sample and a conductive tip (k =42 N m^{-1}, Pt/Ir coated from NanoSensors). By this way, images of the distribution of the piezoelectric response both out-of-plane (OP) and in-plane (IP) were obtained, where z and x are the directions normal to the sample surface and perpendicular to the cantilever, respectively. Remnant local piezoelectric hysteresis loops were measured in the films on STO and LSMO/STO substrates. To minimize electrostatic contributions between cantilever and surface, these measurements were performed in the strong indentation regime, with tip-surface forces around 100-200 nN and stiff cantilevers.

2.7. Ferroelectric and photovoltaic characterization

Capacitors were fabricated with ~200 nm thick films by the DC sputtering of Pt electrodes on the surfaces of the BFO, 3.125-BFCO and 6.25-BFCO films on Pt/Si, and 12.5-BFCO and 25-BFCO films on LSMO/STO. Very thin Pt top electrodes with an average diameter of ~ 200 μm were deposited on the film surface, which have a light transmission and electrical resistance of ~ 38% and ~ 150 Ω, respectively. An array of capacitors was thus prepared using a shadow mask for the deposition of the top Pt electrodes. The bottom electrode was the $La_{0.7}Sr_{0.3}MnO_3$ (LSMO) coated layer on the (100) $SrTiO_3$ (STO) substrate. Ferroelectric hysteresis loops were measured at low and room temperature with a home-built system, see supplementary information Figure S8.[34] Sinusoidal voltage waves at a frequency of 1 kHz were applied to the samples for these measurements using a HP-8116A pulse generator. The experimental ferroelectric hysteresis loops were recorded with a Tektronix-TDS520 oscilloscope, applying the voltage to the top Pt electrode, while the bottom LSMO electrode was grounded. For the low temperature measurements, the equipment was coupled in a house made cryostat equipped with micro-manipulators. Leakage currents (non-linear contributions) were calculated with a model that considers electrical current proportional to voltage.[35, 36] Ferroelectric hysteresis loops were obtained after subtracting from the experimental loops the non-switching and non-linear leakages contributions. For determining the photo-response of the films, they were illuminated through the top Pt electrodes with a laser light of 520 nm and 15 mW focussed in an area of ~ $1mm^2$. The equipment used to carry out this characterization is shown in Figure S3. Open circuit potential (V_{OC}) was measured as a function of time with and without illumination as well as the time dependence of the short-circuited photocurrent density (J_{SC}) under illumination, using a Palmsense 4 electrochemical interface. Variation of current density with running voltage, J-V curves were measured without light and inducing photo-response under illumination in the films at different temperatures and poling

conditions. From these measurements, Jsc and Voc at the different experimental conditions were deduced. Static (point by point) J-V curves as a function of temperature were also obtained in the films under darkness and illumination and under different poling conditions by a Premier II ferrotester. Incident photon-to-electron conversion efficiency (IPCE) measurements were made based on a commercial apparatus (Newport) with UNIVERSAL ARC LAMP HOUSINGS 500 WATT FAMILY(66902) and using a 300 W Xenon lamp.

3. Results and discussion

3.1. Stress-mediated solution deposition method of thin films

In the fabrication of perovskite thin films, the strain generated by the mismatch between the film and the substrate can be used to produce changes in the perovskite crystal structure, with the consequent tuning of the film properties with respect to the bulk material.[27, 37-42] Hence, ferroelectric perovskite thin films like $BaTiO_3$, $PbTiO_3$ or $BiFeO_3$ have been epitaxially grown on compressive substrates like $SrTiO_3$ (STO) single crystals by physical deposition techniques like PLD. However, only scarce reports describing the formation and stabilization of HP metastable perovskite thin films can be found in the literature.[21, 25, 41] A key factor to achieve this goal is related to the lattice mismatch compressive strain imposed to the thin film by the STO substrate during the formation of the metastable perovskite. Under these growth conditions, the metastable perovskite film can be far from ambient pressure and much closer to the high pressures used to prepare powders and bulk ceramics.[17, 20] As a consequence, the fabrication of HP perovskite thin films has been made on compressive substrates like STO, but it has been unfeasible on non-compressive substrates like those inducing in the film a tensile stress like Pt-coated silicon.[43] Processing difficulties intensify if these HP metastable perovskite thin films are fabricated by solution processing methods, such as Chemical Solution Deposition (CSD). [44-46] Although this method is a promising scalable deposition technique to prepare the large-area, low-cost

coatings demanded in many applications (*e.g.,* self-powered smart devices or photovoltaic solar panels[28]), these HP metastable perovskite thin films have never been fabricated by CSD. The latter is mainly due to the initial tensile stresses induced in the solution deposited layer (thin film shrinking) upon the release of solvents and organics during drying and pyrolysis.[47] Then, during the annealing at higher temperatures applied for the film crystallization, there is a lattice mismatch between the perovskite layer and the substrate, which imposes the thin film to tension when deposited on substrates like silicon, and to compression when substrates like STO are used. This mismatch induces an epitaxial strain in the perovskite film for the latter substrates, which continues during cooling due to the dilatation coefficient difference between the compressive substrate and the just crystallized perovskite film. However, this stress has not been large enough to stabilize in the film HP metastable perovskite phases when fabricated by the CSD method.[37, 38, 47, 48] .

Therefore, taking into account the distintive behavior of CSD thin films during annealing, we report here a new solution processing strategy to fabricate and stabilize HP metastable perovskite thin films. The method is based on the application of an external compressive stress to the deposited layer during crystallization. This external stress adds to the stress already imposed by the STO substrate, permitting the formation and stabilization of HP metastable perovskite.

The processing method is schematically shown in **Figure 1**. Here, the application of an external force during the thermal treatment of the solution deposited layer, results in the deformation, ϵ_f, of the sample, which gives rise a high compressive stress in the whole sample. The external compressive stress applied to the sample opposes to the inherent tensile stresses produced in the solution layer during heating up to the temperature of crystallization.[37, 38, 47, 49] The external compressive stress facilitates the diffusion and ordering of the ions when the crystallization temperature is reached and just when the HP

crystal phase becomes thermodynamically stable under these temperature and pressure conditions. Finally, cooling the perovskite film sets the substrate in a compression mode, [38, 47] which is increased even more with the externally applied compression force from the sample holder. As a result, the sample reaches the HP conditions required for the stabilization of the HP ferroelectric perovskites in CSD thin films.

The deformation of the sample produced by the applied force is calculated with the formula: $€_f = 6\ d\ h\ /\ L^2$ (Figure 1), where $€_f$ is proportional to the displacement in height of the sample, *d*, and to the thickness of the sample, *h*, and it is inversely proportional to the length squared of the sample, L^2 (see Figures 1). By using the sample holder shown in Figure 1d and 1e, a deformation of ~4‰, calculated taking into account the Young's modulus of $BiFeO_3$, was applied to a sample formed by a ~50 nm thick film on a STO substrate (substrate thickness of ~1 mm). This deformation is equivalent to a compressive stress close to 1 GPa, which is added to the stress coming from the substrate, also in the GPa range.[37, 38, 47, 50] This strategy places the solution deposited film during crystallization under the boundary conditions needed to stabilize these HP metastable perovskite phases.[17, 19, 20]

3.2. Proof of concept on ferroelectric HP metastable perovskite thin films

We demonstrate this stress-mediated solution deposition method in thin films of the HP $BiFe_{1-x}Cr_xO_3$ (BFCO) perovskites with large amounts of chromium, which, to our knowledge, have never been prepared before by CSD on any substrate. [31, 44-46, 51-53]

Films of the single ferroelectric BFCO perovskite phase can be obtained on (tensile) Pt-coated silicon substrates by conventional CSD process (without the application of an external stress) only for small amounts of chromium, ≤ 6 mol%. However, the incorporation of larger amounts of chromium into the BFCO perovskite films (compositions for which the perovskite becomes a metastable phase) is not possible when silicon substrates are used. Neither applying the external compressive stress devised in this work, it would be possible. This is

because at the temperatures at which these perovskites crystallize (≥ 500ºC), the silicon substrate would be in its plastic region and the external stress applied to the whole sample would be only used to producing the plastic deformation of the substrate.

Figure 2 shows the XRD patterns and the ferroelectric hysteresis loops obtained in these BFCO films on Pt/Si with low amounts of chromium. They show a rhombohedral structure and a random orientation, in addition to a good ferroelectric response. However, note that we have not been able to stabilize the ferroelectric perovskite in these films for chromium contents over 6 mol%. In this case, the highest XRD peak recorded corresponds to a broad reflection at $2\theta \sim 27.84°$, which can be assigned to crystal structures close to those of the $BiCrO_3$, Bi_2O_3, $Bi_7CrO_{12.5}$ or $Bi_{25}CrO_{40}$ phases.[45, 54, 55]

When these solutions are directly deposited on STO substrates, the films of the pure $BiFeO_3$ (BFO) easily crystallize, without applying an external stress and with a strong preferred orientation along the (0 1 2) direction. This is because of the epitaxial strain produced by the mismatch between the STO substrate and the perovskite layer (**Figure 3a)**.[40, 50] However, these levels of compression, only induced by the substrate, are not enough to stabilize in these CSD films the single HP metastable BFCO perovskite phase with large amounts of chromium (**Figures 3b and 3c**). For that, it is necessary to induce an additional compressive stress during the film fabrication, like that externally applied by the stress-mediated solution deposition method shown in Figure 1. It should be noted that as the amount of chromium in the perovskite increases, the formation of the single HP metastable perovskite phase requires a higher crystallization temperature.[17] Thus, whereas the temperature needed for the crystallization under stress of the HP 12.5-BFCO film is only of 500ºC, to attain under stress the single perovskite phase in the HP 25-BFCO film needs to increase the crystallization temperature up to 600ºC (Figures 3b and 3c). And, for the largest amount of chromium, x =

0.5 (50-BFCO film), the crystallization of the HP metastable perovskite is not achieved in the film at any temperature by using this stress-mediated solution deposition method.

The high resolution XRD reciprocal space maps (rsm) of these films carried out around the (2 0 0) and (-1 0 3) STO reflections (**Figures 4a to 4f**) also prove the formation of these HP metastable BFCO perovskite films with a strong (0 1 2) preferred orientation. **Table 1** shows the in-plane and out-of-plane lattice constants obtained from these data for the HP 12.5-BFCO and HP 25-BFCO films, in comparison with the cell parameters measured for the pure BFO film and the STO substrate. The in-plane lattice constant (*a*) of all the films is close to that of the STO substrate. However, the out-of-plane lattice constant (*c*) is higher than that of the substrate and increases as chromium is introduced into the B-site of the perovskite. This results in an increase in the cell volume, which has associated a decrease in the bandgap of the film. (Table 1).[16, 21, 41, 55, 56]

This reduction of the bandgap with the increase of the chromium content is attained for both types of films: on Pt/Si and on STO (**Figure 5)**. However, it should be noted the appreciable difference in bandgap between the pure $BiFeO_3$ (BFO) film when deposited on Pt/Si or on STO. Whereas the former presents a maximum of light absorption in the visible range, at ~ 430 nm, with a bandgap of Eg ~ 2.84 eV, the latter shows a maximum light absorption in the near ultraviolet range, at λ ~ 390 nm, with Eg ~ 3.00 eV.[51, 57] This variation in the bandgap value has been reported to be probably due to the structural strain induced in epitaxially grown (or strong preferred oriented) $BiFeO_3$ thin films on compressive substrates like STO, $LaAlO_3$ or $YAlO_3$ (see Table S1). Although the compressive strain produced by these substrates can be able to stabilize in the film a non-equilibrium phase like the quasi-tetragonal $BiFeO_3$ or, in this work, the HP metastable $BiFe_{1-x}Cr_xO_3$ perovskite, the bandgap and charge transfer excitations are blue-shifted by around +0.3 eV, thus giving rise optical properties less attractive for solar applications.[51, 57, 58]

Just considering this behavior, the incorporation of large amounts of chromium in the random oriented BFCO perovskite thin films would be more favorable for a strong reduction of the bandgap than introducing this chromium in epitaxial or strongly oriented perovskite films. But as shown before, chromium contents over 6 mol% are not allowed for the random oriented BFCO perovskite films (Figure 2a).[17, 44, 45] Only, the compressive strain induced in the film by the STO substrate joined to the external compressive stress applied to the sample places the solution deposited film during crystallization under the boundary conditions needed to stabilize the HP metastable BFCO perovskite phase with large amounts of chromium.

In addition, it should be noted that the narrow bandgap reported for epitaxial $BiFe_{0.5}Cr_{0.5}$ perovskite films grown by PLD is associated to a Fe^{2+}/Cr^{4+} cationic ordering.[21] This ordering is hindered in BFCO perovskites outside this composition. Thus, we did not observe the (1/2 1/2 1/2) reflection corresponding to the supperlattice, neither in the XRD pattern of the HP 12.5BFCO film nor in that of the HP 25BFCO film.

The lowest Eg value has been obtained in this work for the HP 12.5-BFCO film (Eg ~ 2.57 eV), which has the largest unit cell volume (Table 1). Actually, the same unit cell volume is obtained for the HP 25-BFCO film, which is consistent with its Eg value of ~ 2.59 eV, very close to that of the HP 12.5-BFCO film (see Table 1). In the case of the HP 25-BFCO film, the slightly lower optical absorption measured is produced by the larger porosity of this film, which increases the scattering of the light by the film surface. This porosity is observed in the plan-view and cross-section FEGSEM images of **Figures 6a to 6d**. The EDX elemental mapping of the films (Figures 6e to 6j) indicates a homogeneous distribution of chromium, iron and bismuth. However, the largest amount of black regions observed in the HP 25-BFCO film is an indication of no emission of the former elements, which is consistent with the larger porosity observed in the HP 25-BFCO film than in the HP 12.5-BFCO film. Areas with

an accumulation of cations, which could be associated to second non-perovskite phases are not detected in the films.

Figures 7 and S2 show the Piezoresponse Force Microscopy (PFM) analysis of the HP 12.5-BFCO and HP 25-BFCO films. The topography images of both films indicate similar size of their grains (Figures 7a and 7b), which are all piezoelectric according to the out-of-plane amplitude (Figures 7c and 7d) and phase (Figures 7e and 7f) PFM images.[31, 59] A larger porosity is observed in the topography image of the HP 25-BFCO film, in agreement with the FEGSEM and EDX results of Figure 6. Regions of the film surfaces without piezoresponse, which would be representative of secondary non ferroelectric phases, are not observed by PFM. Figures 7g and 7h display representative local piezoelectric hysteresis loops measured in different grains of the films, which proves the ferroelectric character of these HP BFCO perovskite films prepared by the stress-mediated CSD method developed in this work.

3.3. Ferroelectric and photovoltaic properties of the HP BFCO perovskite films

The ferroelectric and photovoltaic responses of these HP BFCO perovskite films were obtained in devices fabricated with ~ 200 nm thick films as the only light absorber, which were deposited on $La_{0.7}Sr_{0.3}MnO_3$ coated (100) $SrTiO_3$ (LSMO/STO) substrates, and with very thin Pt top electrodes (see **Figures 8 and S3**). Figures 8b and 8c shows the ferroelectric hysteresis loops measured at low temperature in this device for the HP 12.5-BFCO film. High values of remnant polarization are obtained (P_R ~ 40 μC cm^{-2}), which are only slightly lower than those reported for pure $BiFeO_3$ films.[31, 60] This decrease in P_R supports the incorporation of chromium into the HP metastable BFCO perovskite films,[21, 61] since the reduction of the asymmetry of the perovskite cell with the chromium content (Table 1) should be accompanied by a diminution in the ferroelectric response. Besides, the increase of the non-ferroelectric contributions (conductivity and leakages) observed in the hysteresis loop of

the device fabricated with the HP 25-BFCO film (**Figure S4**a) is associated to the larger porosity of this film.[62]

The not polarized device exhibits photovoltaic response at room temperature, as shown in Figures. 8d to 8f. A short circuit current density (J_{SC}) and an open circuit voltage (V_{OC}) of ~ 6×10^{-3} mA cm^{-2} and ~ 0.10 V, respectively, are obtained (Figure 8f). For a general comparison, the $V_{OC} \times J_{SC}$ value may indirectly reflect the out-put power of the device.[3] Thus, an out-put power of ~ 0.6 μW cm^{-2} is obtained for the not-polarized film under illumination. This value is high compared with the results reported in the literature for conventional ferroelectric perovskite materials (*i.e.*, non HP metastable ferroelectric perovskites).[3, 7] These out-put power values are in the range of the micropower electricity required in self-powered smart devices to work,[2, 3] thus showing the potential of these HP ferroelectric perovskite thin films for the harvesting of light energy. Furthermore, the device after the polarization of the film shows higher J_{SC} and V_{OC} values, ~ 40×10^{-3} mA cm^{-2} and ~ 0.16 V, respectively (Figure 8g). From these results, an out-put power of ~ 6.4 μW cm^{-2} is achieved, which is an order of magnitude higher than the out-put power of the not-polarized device. This is mainly due to the increase of J_{SC} resulting from the reduction of the recombination of the charge carriers in the polarized film and also to the reduction of the ohmic resistance of the film after switching,[63] which is supported by the increase of the Voc measured at room temperature in the polarized film device. This phenomenon is associated to the ferroelectric domains present in the polarized film, which work as internal junctions for the separation of the photoexcited electron and hole pairs.[28, 64] This is an important outcome from our point of view, since it demonstrates the coupling effect between the ferroelectric and the photovoltaic properties[6, 12, 28, 65, 66] in these HP metastable BFCO perovsite thin films. The Incident Photon to Current Efficiency (IPCE) as a function of wavelength of these devices, using the HP metastable BFCO perovskite films as the only

light absorber, is shown in Figure S4h. IPCE is of the same order of magnitude than that reported for $BiFeO_3$ based photovoltaic devices with a similar device configuration.[55] Although it is low for using these thin films directly in solar cells, there is still room for improving. Thus, simply considering a planar capacitor configuration, using transparent and high conductive electrodes would increase the amount of light arriving at the film.[6, 28, 65] Besides, decreasing the film thickness (distance between electrodes) would produce an increase in V_{OC}. Work is currently in progress in our group to optimize these properties in these films.

Our goal here has been to demonstrate the potential of this stress-mediated solution deposition method for the synthesis of ferroelectric HP metastable $BiFeO_3$ based perovskite phases in thin film form as candidates for self-powered multifunctional devices.

4. Conclusions

We have demonstrated for the first time, a novel stress-mediated Chemical Solution Deposition method for the preparation of ferroelectric HP metastable $BiFeO_3$ based perovskite films. The method overcomes the complexity of the fabrication processes under the severe conditions required for the synthesis and stabilization of powders and bulk ceramics of these phases, and gives access to prepare these perovskites in thin film form. This approach has been demonstrated for films of the HP metastable $BiFe_{1-x}Cr_xO_3$ perovskite with large amounts of chromium. The application of an external compressive stress to the thin film layer combined with the strength directly induced by the compressive $SrTiO_3$ substrate produce a high film deformation during the thin film crystallization. This provokes the incorporation of chromium into the perovskite cell and the stabilization of the metastable phase. HP metastable $BiFe_{1-x}Cr_xO_3$ perovskite films with a strong (0 1 2) preferred orientation are successfully prepared with substitutions of iron by chromium up to a 25

mol%. The films have a narrow bandgap (Eg ~ 2.57 eV), while preserving a very good ferroelectric response (P_R ~ 40 μC cm^{-2}). In addition, a large out-put power of ~ 6.4 μW cm^{-2} is obtained in the device fabricated with the polarized films. The later demonstrates the potential of these materials to be applied as light harvesters and, given the ferroelectric character of the films, for their integration in self-powered multifunctional systems. The successful stabilization of these ferroelectric HP perovskites in thin film form indicates that there is still room for improving the functionality of these materials by an accurate control of the perovskite structure and an appropriate design of the device. In addition, the non-toxicity, stability and long cycle life of these ferroelectric HP metastable perovskite thin films are also important advantages for their use in wireless self-powered smart systems.

Associated content. *Supporting Information.*

Corresponding author. *M. Lourdes Calzada* – Instituto de Ciencia de Materiales de Madrid (ICMM). Consejo Superior de Investigaciones Científicas (CSIC). C/ Sor Juana Inés de la Cruz 3, Cantoblanco. Madrid 28049. Spain. E-mail: lcalzada@icmm.csic.es

Acknowledgment. This work has been financed by Spanish Projects PID2019-104732RB-I00, MAT2016-76851-R, MAT2017-91772-EXP (AEI/FEDER, UE) and RTI2018-096918-B-C41. I.B. acknowledges financial support from the Ramón&Cajal Spanish Programm. We thank Dr. M.Coll and P.Machado for the deposition of LSMO layers on the STO substrates (Instituto de Ciencia de Materiales de Barcelona ICMAB-CSIC). M.L.-C. and H.X. acknowledges the support from Spanish MINECO for the grant GraPErOs (ENE2016-79282-C5-2-R), the OrgEnergy Excellence Network CTQ2016-81911- REDT, the Agència de Gestiód'Ajuts Universitaris i de Recerca (AGAUR) for the support to the consolidated Catalonia research group 2017 SGR 329 and the Xarxa de Referència en Materials Avançats per a l'Energia

(Xarmae). ICN2 is supported by the Severo Ochoa program from Spanish MINECO (Grant No. SEV-2017-0706) and is funded by the CERCA Programme / Generalitat de Catalunya.

References

[1] G. Turner, Global Renewable Energy Market Outlook 2013, Bloomberg New Energy Finance, 2014, https://www.bnef.com/insightdowmload/7526/pdf, 2014.
[2] Y. Bai, H. Jantunen, J. Juuti, Energy Harvesting Research: The Road from Single Source to Multisource, Advanced Materials 30(34) (2018).
[3] Y. Bai, P. Tofel, J. Palosaari, H. Jantunen, J. Juuti, A Game Changer: A Multifunctional Perovskite Exhibiting Giant Ferroelectricity and Narrow Bandgap with Potential Application in a Truly Monolithic Multienergy Harvester or Sensor, Advanced Materials 29(29) (2017).
[4] H. Huang, J.F. Scott, Ferroelectric materials for energy applications, Wiley-VCH Verlag GMBh&Co. KGaA, Weinheim, Germany, 2018.
[5] W.X. Gao, R. Brennan, Y. Hu, M. Wuttig, G.L. Yuan, E. Quandt, S.Q. Ren, Energy transduction ferroic materials, Materials Today 21(7) (2018) 771-784.
[6] C. Paillard, X.F. Bai, I.C. Infante, M. Guennou, G. Geneste, M. Alexe, J. Kreisel, B. Dkhil, Photovoltaics with Ferroelectrics: Current Status and Beyond, Advanced Materials 28(26) (2016) 5153-5168.
[7] Y. Ji, K. Zhang, Z.L. Wang, Y. Yang, Piezo-pyro-photoelectric effects induced coupling enhancement of charge quantity in BaTiO3 materials for simultaneously scavenging light and vibration energies, Energy & Environmental Science 12(4) (2019) 1231-1240.
[8] N. Ma, K. Zhang, Y. Yang, Photovoltaic-Pyroelectric Coupled Effect Induced Electricity for Self-Powered Photodetector System, Advanced Materials 29(46) (2017).
[9] Y. Bai, T. Siponkoski, J. Perantie, H. Jantunen, J. Juuti, Ferroelectric, pyroelectric, and piezoelectric properties of a photovoltaic perovskite oxide, Applied Physics Letters 110(6) (2017).
[10] Y. Ji, K. Zhang, Y. Yang, A One-Structure-Based Multieffects Coupled Nanogenerator for Simultaneously Scavenging Thermal, Solar, and Mechanical Energies, Advanced Science 5(2) (2018).
[11] Y. Bai, G. Vats, J. Seidel, H. Jantunen, J. Juuti, Boosting Photovoltaic Output of Ferroelectric Ceramics by Optoelectric Control of Domains, Advanced Materials 30(43) (2018).
[12] G. Catalan, J.F. Scott, Physics and Applications of Bismuth Ferrite, Advanced Materials 21(24) (2009) 2463-2485.
[13] S.Y. Yang, L.W. Martin, S.J. Byrnes, T.E. Conry, S.R. Basu, D. Paran, L. Reichertz, J. Ihlefeld, C. Adamo, A. Melville, Y.H. Chu, C.H. Yang, J.L. Musfeldt, D.G. Schlom, J.W. Ager, R. Ramesh, Photovoltaic effects in BiFeO3, Applied Physics Letters 95(6) (2009).
[14] P. Baettig, N.A. Spaldin, Ab initio prediction of a multiferroic with large polarization and magnetization, Applied Physics Letters 86(1) (2005).
[15] A.R. Akbashev, A.R. Fridkin, J.E. Spanier, Semiconducting and photovoltaic ferroelectrics, in: M. Algueró, J.M. Gregg, L. Mitoseriu (Eds.)2016.
[16] G. Chen, J. Chen, W.J. Pei, Y.M. Lu, Q.F. Zhang, Q. Zhang, Y.B. He, Bismuth ferrite materials for solar cells: Current status and prospects, Materials Research Bulletin 110 (2019) 39-49.
[17] A.A. Belik, Polar and nonpolar phases of BiMO3: A review, Journal of Solid State Chemistry 195 (2012) 32-40.
[18] X.S. Xu, J.F. Ihlefeld, J.H. Lee, O.K. Ezekoye, E. Vlahos, R. Ramesh, V. Gopalan, X.Q. Pan, D.G. Schlom, J.L. Musfeldt, Tunable band gap in Bi(Fe1-xMnx)O-3 films, Applied Physics Letters 96(19) (2010).
[19] M.R. Suchomel, C.I. Thomas, M. Allix, M.J. Rosseinsky, A.M. Fogg, M.F. Thomas, High pressure bulk synthesis and characterization of the predicted multiferroic Bi(Fe1/2Cr1/2)O-3, Applied Physics Letters 90(11) (2007).

[20] C. Goujon, C. Darie, M. Bacia, H. Klein, L. Ortega, P. Bordet, High pressure synthesis of BiCrO3, a candidate for multiferroism, 21st AIRAPT/45th EHPRG International Conference on High Pressure Science and Technology, Univ Catania, Dept Phys Astronomy, Catania, ITALY, 2007.
[21] R. Nechache, C. Harnagea, S. Li, L. Cardenas, W. Huang, J. Chakrabartty, F. Rosei, Bandgap tuning of multiferroic oxide solar cells, Nature Photonics 9(1) (2015) 61-67.
[22] P. Baettig, C. Ederer, N.A. Spaldin, First principles study of the multiferroics BiFeO3, Bi2FeCrO6, and BiCrO3: Structure, polarization, and magnetic ordering temperature, Physical Review B 72(21) (2005).
[23] J. Ricote, D. Chateigner, L. Pardo, M. Alguero, J. Mendiola, M. Calzada, Quantitative analysis of preferential orientation components of ferroelectric thin films, Ferroelectrics 241(1-4) (2000) 167-174.
[24] R. Jiménez, M.L. Calzada, M.L. Mendiola, Preferred orientation of solution derived (Pb,Ca)TiO3 thin films on SrTiO3 and MgO, in: E. Colla, D. Damjanovic, N. Setter (Eds.) Eleventh IEEE International Symposium on Applications of ferroelectrics, Eleventh IEEE International Symposium on Applications of Ferroelectrics, Montreux, Switzerland, 1998, pp. 155-158.
[25] J.H. Lee, X. Ke, R. Misra, J.F. Ihlefeld, X.S. Xu, Z.G. Mei, T. Heeg, M. Roeckerath, J. Schubert, Z.K. Liu, J.L. Musfeldt, P. Schiffer, D.G. Schlom, Adsorption-controlled growth of BiMnO3 films by molecular-beam epitaxy, Applied Physics Letters 96(26) (2010).
[26] D.G. Schlom, L.Q. Chen, C.J. Fennie, V. Gopalan, D.A. Muller, X.Q. Pan, R. Ramesh, R. Uecker, Elastic strain engineering of ferroic oxides, Mrs Bulletin 39(2) (2014) 118-130.
[27] J.H. Haeni, P. Irvin, W. Chang, R. Uecker, P. Reiche, Y.L. Li, S. Choudhury, W. Tian, M.E. Hawley, B. Craigo, A.K. Tagantsev, X.Q. Pan, S.K. Streiffer, L.Q. Chen, S.W. Kirchoefer, J. Levy, D.G. Schlom, Room-temperature ferroelectricity in strained SrTiO3, Nature 430(7001) (2004) 758-761.
[28] I. Bretos, R. Jimenez, J. Ricote, M.L. Calzada, Synthesis by Low Temperature Solution Processing of Ferroelectric Perovskite Oxide Thin Films as Candidate Materials for Photovoltaic Applications, Future of Semiconductor Oxides in Next-Generation Solar Cells (2018) 45-81.
[29] D. Perez-Mezcua, R. Sirera, R. Jimenez, I. Bretos, C. De Dobbelaere, A. Hardy, M.K. Van Bael, M. Lourdes Calzada, A UV-absorber bismuth(III)-N-methyldiethanolamine complex as a low-temperature precursor for bismuth-based oxide thin films, Journal of Materials Chemistry C 2(41) (2014) 8750-8760.
[30] I. Bretos, R. Jiménez, J. Ricote, R. Sirera, M. Calzada, Flexible photoferroelectric thin films of BiFeO3 by solution processing from tailored low-temperature precursors, Advanced Functional Materials (2020).
[31] C. Gutierrez-Lazaro, I. Bretos, R. Jimenez, J. Ricote, H. El Hosiny, D. Perez-Mezcua, R.J. Jimenez Rioboo, M. Garcia-Hernandez, M.L. Calzada, Solution Synthesis of BiFeO3 Thin Films onto Silicon Substrates with Ferroelectric, Magnetic, and Optical Functionalities, Journal of the American Ceramic Society 96(10) (2013) 3061-3069.
[32] A. Kumar, N.J. Podraza, S. Denev, J. Li, L.W. Martin, Y.H. Chu, R. Ramesh, R.W. Collins, V. Gopalan, Linear and nonlinear optical properties of multifunctional PbVO3 thin films, Applied Physics Letters 92(23) (2008).
[33] A. Kumar, R.C. Rai, N.J. Podraza, S. Denev, M. Ramirez, Y.-H. Chu, L.W. Martin, J. Ihlefeld, T. Heeg, J. Schubert, D.G. Schlom, J. Orenstein, R. Ramesh, R.W. Collins, J.L. Musfeldt, V. Gopalan, Linear and nonlinear optical properties of BiFeO3, Applied Physics Letters 92(12) (2008).
[34] C. Alemany, R. Jimenez, J. Revilla, J. Mendiola, M. Calzada, Pulsed hysteresis loops on ferroelectric thin films, Journal of Physics D-Applied Physics 32(17) (1999) L79-L82.

[35] R. Jimenez, C. Alemany, M. Calzada, A. Gonzalez, J. Ricote, J. Mendiola, Processing effects on the microstructure and ferroelectric properties of strontium bismuth tantalate thin films, Applied Physics a-Materials Science & Processing 75(5) (2002) 607-615.
[36] D. Rivero, L. Pardo, R. Jiménez, Instalación para Medir el Lazo de Histéresis y las Corrientes de Conmutación en Láminas Delgadas de Materiales Ferroeléctricos, Revista Cubana de Física 26 (2009) 169-173.
[37] A. Seifert, F.F. Lange, J.S. Speck, EPITAXIAL-GROWTH OF PBTIO3 THIN-FILMS ON (001)SRTIO3 FROM SOLUTION PRECURSORS, Journal of Materials Research 10(3) (1995) 680-691.
[38] M. Calzada, R. Jimenez, Y. Mendiola, Orientation of sol-gel prepared (Pb,Ca)TiO3 thin films, Boletin De La Sociedad Espanola De Ceramica Y Vidrio 38(3) (1999) 227-230.
[39] A. Chen, H. Zhou, Y. Zhu, L. Li, W. Zhang, J. Narayan, H. Wang, Q. Jia, Stabilizing new bismuth compounds in thin film form, Journal of Materials Research 31(22) (2016) 3530-3537.
[40] J. Manuel Vila-Fungueirino, A. Gomez, J. Antoja-Lleonart, J. Gazquez, C. Magen, B. Noheda, A. Carretero-Genevrier, Direct and converse piezoelectric responses at the nanoscale from epitaxial BiFeO3 thin films grown by polymer assisted deposition, Nanoscale 10(43) (2018) 20155-20161.
[41] R. Nechache, C. Harnagea, L.-P. Carignan, O. Gautreau, L. Pintilie, M.P. Singh, D. Menard, P. Fournier, M. Alexe, A. Pignolet, Epitaxial thin films of the multiferroic double perovskite Bi2FeCrO6 grown on (100)-oriented SrTiO3 substrates: Growth, characterization, and optimization, Journal of Applied Physics 105(6) (2009).
[42] M. Alguero, A. Bushby, M. Reece, R. Poyato, J. Ricote, M. Calzada, L. Pardo, Stress-induced depolarization of (Pb, La)TiO3 ferroelectric thin films by nanoindentation, Applied Physics Letters 79(23) (2001) 3830-3832.
[43] R. Nechache, W. Huang, S. Li, F. Rosei, Photovoltaic properties of Bi2FeCrO6 films epitaxially grown on (100)-oriented silicon substrates, Nanoscale 8(6) (2016) 3237-3243.
[44] Z.Y. Zhong, S.K. Singh, Y. Sugiyama, H. Ishiwara, Ferroelectric Properties of Cr-Doped BiFeO3 Films Crystallized below 500 degrees C, Japanese Journal of Applied Physics 48(10) (2009).
[45] H. Deng, H.M. Deng, P.X. Yang, J.H. Chu, Effect of Cr doping on the structure, optical and magnetic properties of multiferroic BiFeO3 thin films, Journal of Materials Science-Materials in Electronics 23(6) (2012) 1215-1218.
[46] C.H. Nie, S.F. Zhao, Y.L. Bai, Q.S. Lu, The ferroelectric photovoltaic effect of BiCrO3/BiFeO3 bilayer composite films, Ceramics International 42(12) (2016) 14036-14040.
[47] B.A. Tuttle, J.A. Voigt, T.J. Garino, D.C. Goodnow, R.W. Schwartz, D.L. Lamppa, T.J. Headley, M.O. Eatough, CHEMICALLY PREPARED PB(ZR,TI)O3 THIN-FILMS - THE EFFECTS OF ORIENTATION AND STRESS, Isaf 92 : Proceedings of the Eighth Ieee International Symposium on Applications of Ferroelectrics (1992) 344-348.
[48] K.T. Miller, C.J. Chan, M.G. Cain, F.F. Lange, EPITAXIAL ZIRCONIA THIN-FILMS FROM AQUEOUS PRECURSORS, Journal of Materials Research 8(1) (1993) 169-177.
[49] M. Alguero, M. Calzada, L. Pardo, E. Snoeck, Combined effect of grain size and tensile stresses on the ferroelectric properties of sol-gel (Pb,La)TiO3 thin films, Journal of Materials Research 14(12) (1999) 4570-4580.
[50] F.F. Lange, Chemical solution routes to single-crystal thin films, Science 273(5277) (1996) 903-909.
[51] P. Chen, N.J. Podraza, X.S. Xu, A. Melville, E. Vlahos, V. Gopalan, R. Ramesh, D.G. Schlom, J.L. Musfeldt, Optical properties of quasi-tetragonal BiFeO3 thin films, Applied Physics Letters 96(13) (2010).

[52] J.K. Kim, S.S. Kim, W.J. Kim, M.H. Park, A.S. Bhalla, R. Guo, Influences of Cr doping on the electrical properties in BiFeO3 thin films, Ferroelectrics Letters Section 33(3-4) (2006) 91-100.
[53] S.K. Singh, K. Sato, K. Maruyama, H. Ishiwara, Cr-doping effects to electrical properties of BiFeO3 thin films formed by chemical solution deposition, Japanese Journal of Applied Physics Part 2-Letters & Express Letters 45(37-41) (2006) L1087-L1089.
[54] H. Deng, H.M. Deng, D.J. Huang, L.P. Zhu, P.X. Yang, Optical properties of BiCrxFe1-xO3 films grown by sol-gel method, 3rd International Photonics and OptoElectronics Meetings, Wuhan, PEOPLES R CHINA, 2010.
[55] P. Machado, M. Scigaj, J. Gazquez, E. Rueda, A. Sanchez-Diaz, I. Fina, M. Gibert-Roca, T. Puig, X. Obradors, M. Campoy-Quiles, M. Coll, Band Gap Tuning of Solution-Processed Ferroelectric Perovskite BiFe1-xCoxO3 Thin Films, Chemistry of Materials 31(3) (2019) 947-954.
[56] Z. Fan, K. Sun, J. Wang, Perovskites for photovoltaics: a combined review of organic-inorganic halide perovskites and ferroelectric oxide perovskites, Journal of Materials Chemistry A 3(37) (2015) 18809-18828.
[57] L. Qiao, S. Zhang, H.Y. Xiao, D.J. Singh, K.H.L. Zhang, Z.J. Liu, X.T. Zu, S. Li, Orbital controlled band gap engineering of tetragonal BiFeO3 for optoelectronic applications, Journal of Materials Chemistry C 6(5) (2018) 1239-1247.
[58] C. Himcinschi, A. Bhatnagar, A. Talkenberger, M. Barchuk, D.R.T. Zahn, D. Rafaja, J. Kortus, M. Alexe, Optical properties of epitaxial BiFeO3 thin films grown on LaAlO3, Applied Physics Letters 106(1) (2015).
[59] N. Salazar, D. Perez-Mezcua, M. Lourdes Calzada, A. Gil, J. Ricote, Ergodicity of fine-grained canonical relaxor ferroelectric (Bi0.5Na0.5)(1-)xBaxTiO3 films, Journal of the American Ceramic Society 102(10) (2019) 5941-5951.
[60] J. Wang, J.B. Neaton, H. Zheng, V. Nagarajan, S.B. Ogale, B. Liu, D. Viehland, V. Vaithyanathan, D.G. Schlom, U.V. Waghmare, N.A. Spaldin, K.M. Rabe, M. Wuttig, R. Ramesh, Epitaxial BiFeO3 multiferroic thin film heterostructures, Science 299(5613) (2003) 1719-1722.
[61] D.H. Kim, H.N. Lee, M.D. Biegalski, H.M. Christen, Large ferroelectric polarization in antiferromagnetic BiFe0.5Cr0.5O3 epitaxial films, Applied Physics Letters 91(4) (2007).
[62] M.M. Samantaray, A. Gurav, E.C. Dickey, C.A. Randall, Electrode Defects in Multilayer Capacitors Part I: Modeling the Effect of Electrode Roughness and Porosity on Electric Field Enhancement and Leakage Current, Journal of the American Ceramic Society 95(1) (2012) 257-263.
[63] I. Bretos, R. Jimenez, C. Gutierrez-Lazaro, I. Montero, M.L. Calzada, Defect-mediated ferroelectric domain depinning of polycrystalline BiFeO3 multiferroic thin films, Applied Physics Letters 104(9) (2014).
[64] S.Y. Yang, J. Seidel, S.J. Byrnes, P. Shafer, C.H. Yang, M.D. Rossell, P. Yu, Y.H. Chu, J.F. Scott, J.W. Ager, III, L.W. Martin, R. Ramesh, Above-bandgap voltages from ferroelectric photovoltaic devices, Nature Nanotechnology 5(2) (2010) 143-147.
[65] A.R. Akbasheb, V.M. Fridkin, J.E. Spanier, Semiconducting and photovoltaic ferroelectrics, in: M. Algueró, J.M. Gregg, L. Mitoseriu (Eds.), Nanoscale Ferroelectrics and Multiferroics. Processing and Characterization Issues, and Nanoscale Effects., John Wiley & Sons Ltd., West Sussec, UK, 2016, pp. 830-850.
[66] A. Bhatnagar, A.R. Chaudhuri, Y.H. Kim, D. Hesse, M. Alexe, Role of domain walls in the abnormal photovoltaic effect in BiFeO3, Nature Communications 4 (2013).

Figure captions

Table 1. Lattice parameters a and c, and unit cell volumes, V, of thin films with an average thickness of ~50 nm and deposited on (1 0 0) $SrTiO_3$ (STO) substrates. These results have been obtained from the high resolution XRD reciprocal space maps (rsm) around the (2 0 0) and (-1 0 3) $SrTiO_3$ reflections. These data have been calculated for the pristine STO substrate and for the BFO film, and for the HP 12.5-BFCO and HP 25-BFCO films. Bandgaps (Eg) measured in these films by spectroscopic ellipsometry are also included.

Figure 1. Scheme of the Chemical Solution Deposition (CSD) method (stress-mediated solution deposition method) used to induce the crystallization and stabilization in thin film form of high-pressure (HP) metastable perovskite phases. The method is based in the application of a controlled force to the solution deposited film, which is maintained during the thermal treatment of crystallization of the film. **(a)** The solution deposition of the film is shown by, *e.g.*, spin-coating. The deposited amorphous layer is subjected to a controlled compressive deformation during the thermal treatment of crystallization, as indicated in **(b)**. Deformation of the sample is calculated with the formula inserted in (b), where ϵ_f = deformation, d = height displacement of the sample, h = sample thickness and L = sample length in between the support bars. **(c)** Photographs of the HP metastable perovskite oxide thin films obtained under these boundary processing conditions on $SrTiO_3$ (STO) substrates. **(d), (e)** Photographs of the home-made stress sample holder, applying a controlled compressive stress to a film on STO.

Figure 2. (a) X-ray diffraction patterns of ~ 50 nm thick BFCO films on Pt-coated (100) silicon substrates (Pt/Si) and with different contents of Cr. The perovskite peaks are indexed in accordance with JCPDS-ICDD card No. 86-1518 for $BiFeO_3$ perovskite. Peak labelled with # corresponds to second phases formed in the BFCO films with Cr contents ≥ 6 mol%. Ferroelectric hysteresis loops (experimental, fitted and switching loops) of the **(b)** 6.25-BFCO, **(c)** 3.125-BFCO and **(d)** BFO thin films on Pt/Si and with a thickness of ~ 200 nm.

Figure 3. X-ray diffraction patters of ~ 50 nm thick BFCO films with 0, 12.5 and 25 mol% Cr, on (100) $SrTiO_3$ (STO) (**(a)** BFO, **(b)** 12.5-BFCO and **(c)** 25-BFCO). Crystallization was carried out without applying external stress or applying a compressive deformation (stress-mediated solution deposition method). The BFCO perovskite phase crystallizes on STO with a high degree of preferred orientation (bismuth iron oxide; JCPDS-ICDD card No. 86-1518). Peak labelled with # is assigned to second phases. Peaks of the $SrTiO_3$ (STO) substrate are indexed according to the cubic strontium titanium oxide; JCPDS-ICDD card No. 35-0734. * can be assigned to the LSMO/STO substrate.

Figure 4. Reciprocal space maps around the (2 0 0) and (-1 0 3) STO reflections for the BFO and BFCO films with an average thickness of ~ 50 nm, deposited on STO: **(a) (b)** 0 mol% Cr (BFO; $BiFeO_3$, **(c) (d)** 12.5 mol% Cr (HP 12.5-BFCO perovskite film) and **(e) (f)** 25 mol% Cr (HP 25-BFCO perovskite film).

Figure 5. **(a)** Refractive index, n(λ), and **(b)** extinction coefficient, k(λ), of the ~ 50 nm thick BFO films on Pt-coated (100) Si substrate (Pt/Si) and on (100) $SrTiO_3$ substrate (STO), and of the ~ 50 nm thick HP 12.5-BFCO and HP 25-BFCO films on STO. **(c)** Optical bandgap, Eg, of the BFCO films as a function of the chromium content (mol% Cr) for the films on Pt/Si and on STO.

Figure 6. Field Emission Gun Scanning Electron Microscopy (FEGSEM) images of the HP metastable BFCO perovskite thin films with 12.5 mol% Cr (HP 12.5-BFCO) and 25 mol% Cr (HP 25-BFCO) deposited on LSMO/STO and with a thickness of ~ 50 nm. **(a)**, **(b)** Cross-section FEGSEM images and **(c)**, **(d)** plan-view FEGSEM images of the HP 12.5-BFCO and HP 25-BFCO films, respectively. Energy Dispersive X-ray (EDX) elemental mapping is shown from (e) to (j): **(e), (f)** Cr-K emission, **(g), (h)** Fe-L emission and **(i), (j)** Bi-M emission, for the HP 12.5-BFCO and HP 25-BFCO films, respectively.

Figure 7. **(a), (b)** Topography, **(c), (d)** out of plane amplitude and **(e), (f)** phase Piezoresponse Force Microscopy (PFM) images, together with **(g), (h)** local piezoelectric loops for the HP 12.5-BFCO and HP 25-BFCO.

Figure 8. Ferroelectric (FE) and photovoltaic (PV) characterization of the ~200 nm thick HP 12.5-BFCO film on a $La_{0.7}Sr_{0.3}MnO_3$ coated (100) $SrTiO_3$ (LSMO/STO) substrate. **(a)** Schematic view of the electrical configuration of the device (planar capacitors) used for the ferroelectric polarization of the films and for the measurement of the photoresponse of the films with/without illumination. Measurements were carried out with the equipment shown in Figure S3. **(b)** Experimental charge current hysteresis loops, J vs E, measured at 138 K in the film without and with illumination. **(c)** Polarization hysteresis loops, P vs E, calculated by the integration of the former J-E loops. **(d)** Open circuit potential (V_{OC}) measured at room temperature (RT) in the not-polarized film as a function of time, with and without illumination. **(e)** Time dependence of short-circuited photocurrent density measured at room temperature (RT) in the not-polarized film and under illumination. **(f)** Variation of current density with voltage, J-V curves, obtained at RT in the not-polarized film, and under darkness and under illumination. **(g)** Variation of current density with voltage, J-V curves, obtained at RT in the polarized film, and under darkness and under illumination.

Table 1

	substrate	~ 500 Å thick films on STO		
	STO	**BFO**	**HP 12.5-BFCO**	**HP 25-BFCO**
a (Å)	3.90(2)	3.88(5)	3.92(2)	3.91(7)
c (Å)	3.90(2)	3.94(3)	3.95(8)	3.95(4)
V (Å^3)	59.32	59.31	60.70	60.70
Eg (eV)	3.75	3.00	2.57	2.59

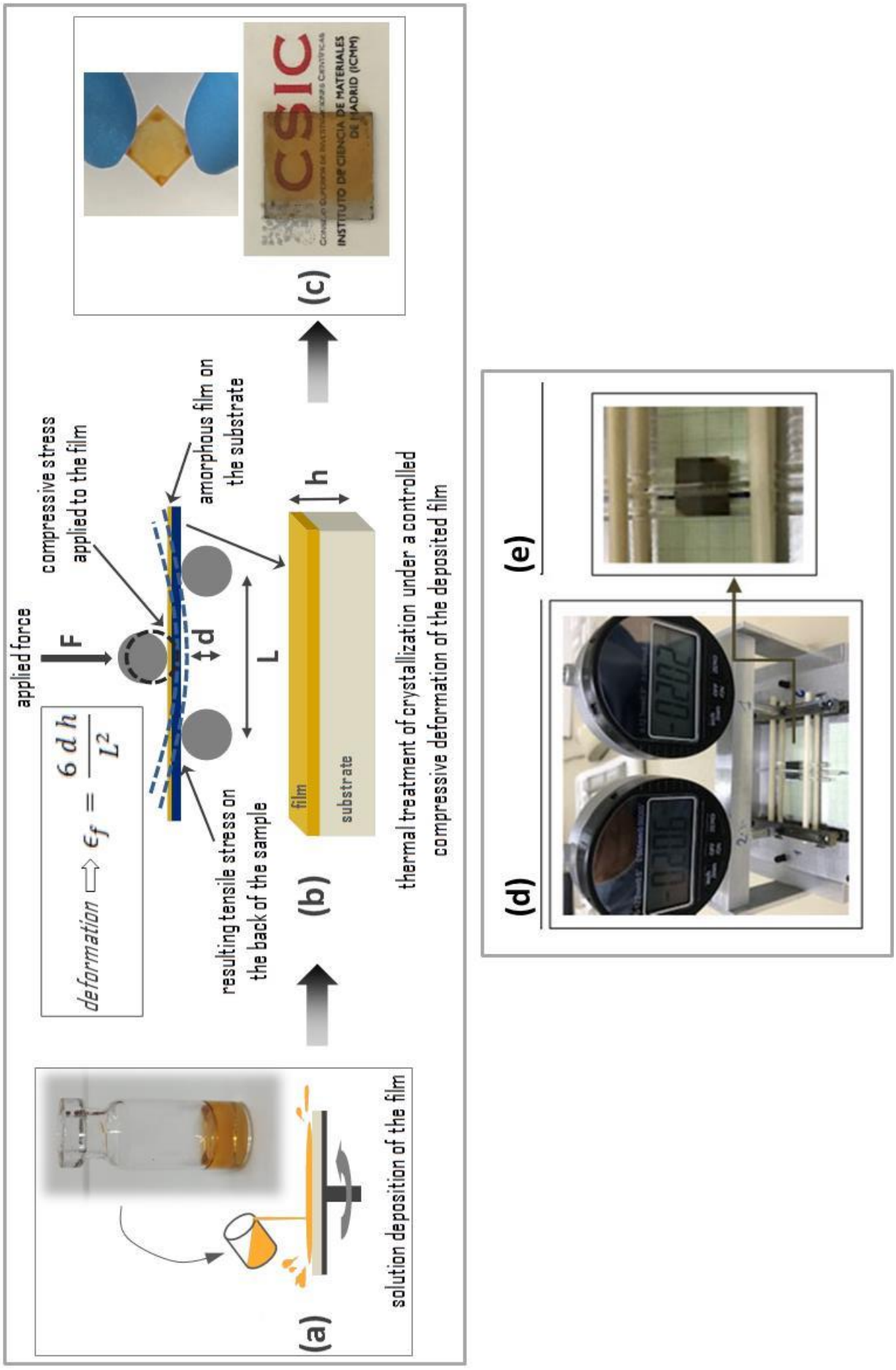
(a)
solution deposition of the film
(b)
thermal treatment of crystallization under a controlled compressive deformation of the deposited film
film
substrate
h
L
d
F
applied force
compressive stress applied to the film
amorphous film on the substrate
resulting tensile stress on the back of the sample
deformation ⇨ $\epsilon_f = \frac{6\,d\,h}{L^2}$
(c)
CSIC
INSTITUTO DE CIENCIA DE MATERIALES DE MADRID (ICMM)
(d)
(e)

Figure 1

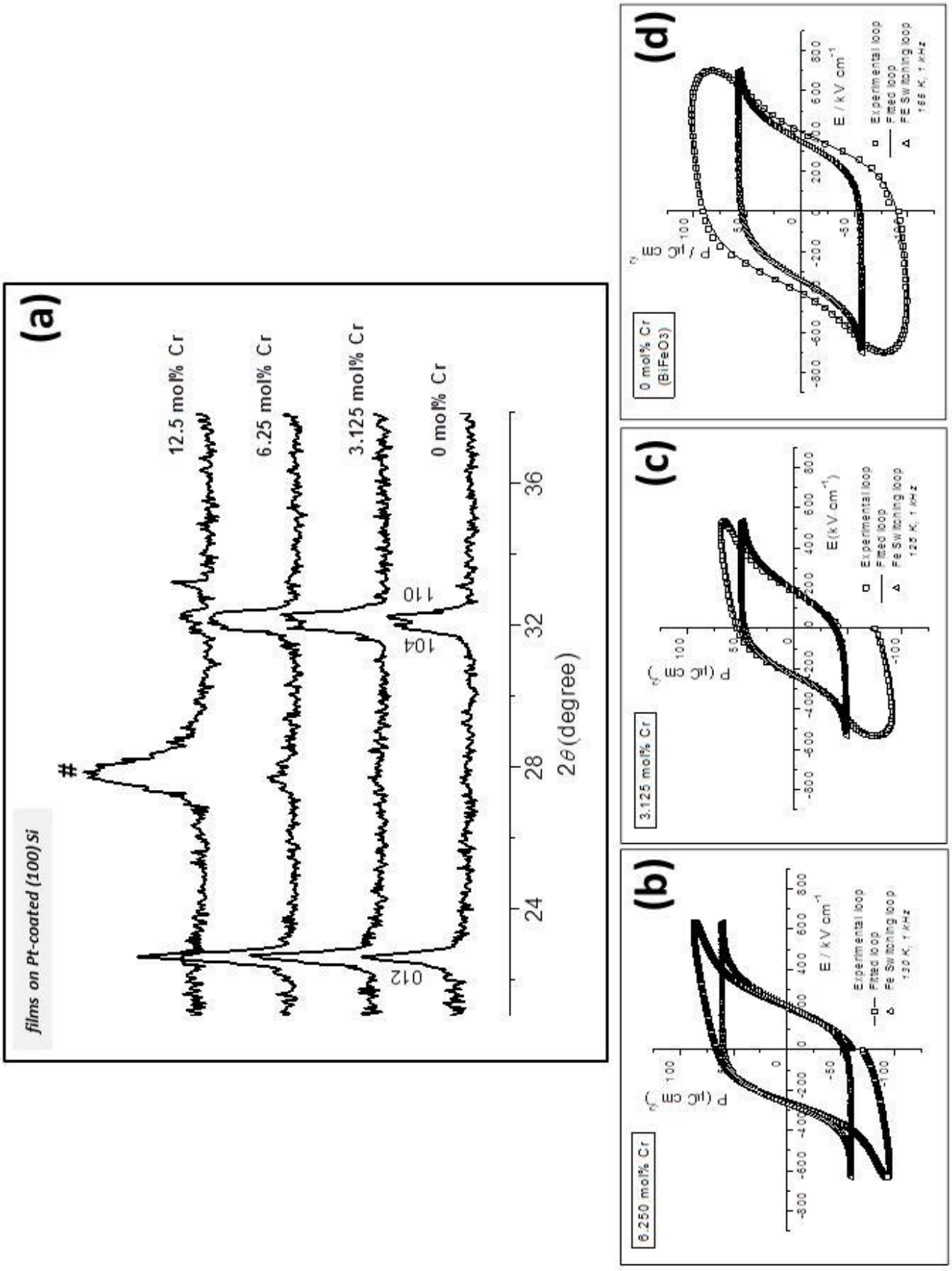
(a)
films on Pt-coated (100) Si
12.5 mol% Cr
6.25 mol% Cr
3.125 mol% Cr
0 mol% Cr
#
012
104
110
24
28
32
36
2θ(degree)
(b)
8.250 mol% Cr
(c)
3.125 mol% Cr
(d)
0 mol% Cr
(BiFeO3)
P (μC cm-2)
E / kV cm-1
E (kV cm-1)
Experimental loop
Fitted loop
Fe Switching loop
125 K, 1 kHz
165 K, 1 kHz

Figure 2

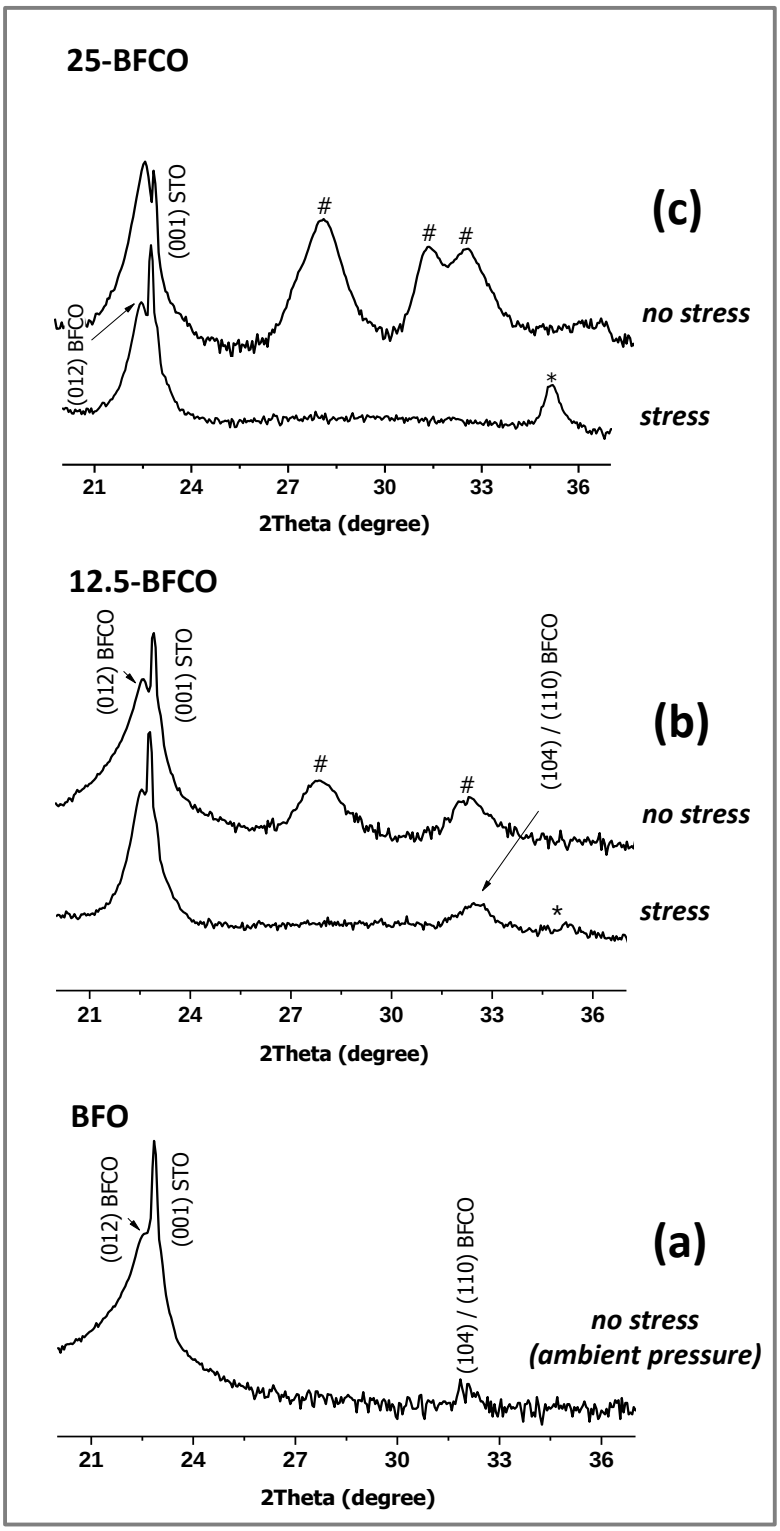
25-BFCO
(001) STO
(012) BFCO
#
#
#
(c)
no stress
stress
*
21
24
27
30
33
36
2Theta (degree)
12.5-BFCO
(012) BFCO
(001) STO
(104) / (110) BFCO
#
#
(b)
no stress
stress
*
21
24
27
30
33
36
2Theta (degree)
BFO
(012) BFCO
(001) STO
(104) / (110) BFCO
(a)
no stress
(ambient pressure)
21
24
27
30
33
36
2Theta (degree)

Figure 3

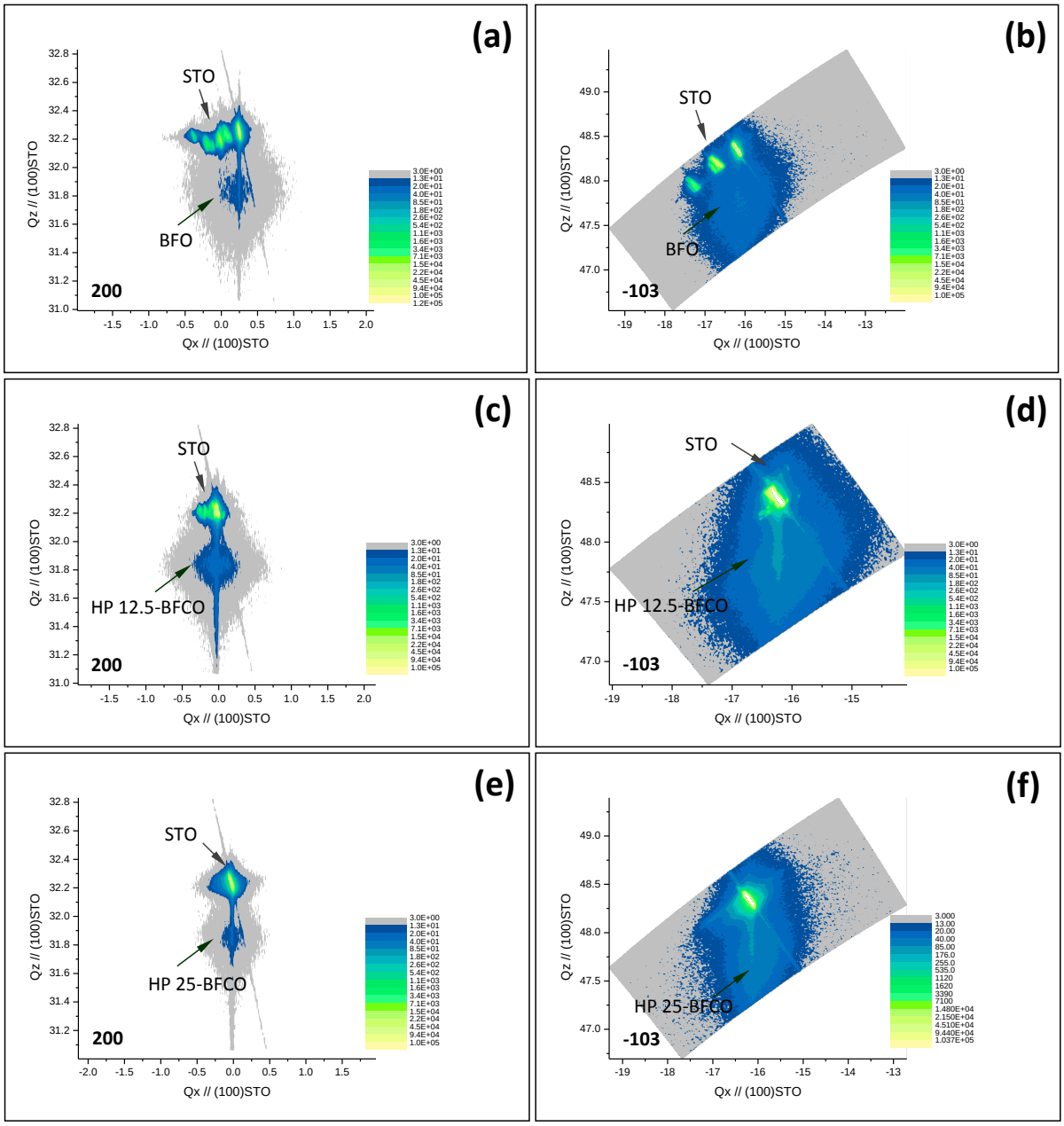
(a)
STO
BFO
200
Qz // (100)STO
Qx // (100)STO
(b)
STO
BFO
-103
Qz // (100)STO
Qx // (100)STO
(c)
STO
HP 12.5-BFCO
200
Qz // (100)STO
Qx // (100)STO
(d)
STO
HP 12.5-BFCO
-103
Qz // (100)STO
Qx // (100)STO
(e)
STO
HP 25-BFCO
200
Qz // (100)STO
Qx // (100)STO
(f)
HP 25-BFCO
-103
Qz // (100)STO
Qx // (100)STO

Figure 4

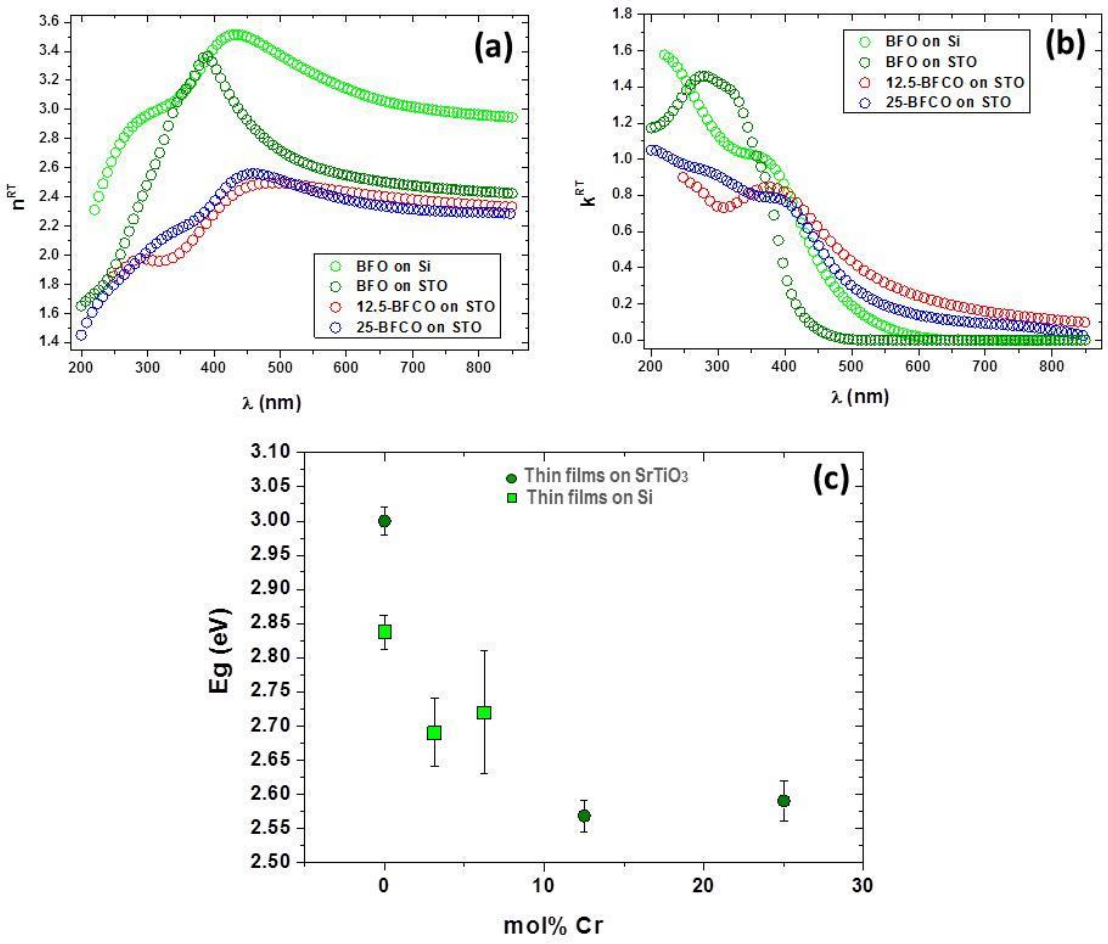
(a)
n^RT
λ (nm)
BFO on Si
BFO on STO
12.5-BFCO on STO
25-BFCO on STO
(b)
k^RT
λ (nm)
BFO on Si
BFO on STO
12.5-BFCO on STO
25-BFCO on STO
(c)
Eg (eV)
mol% Cr
Thin films on SrTiO3
Thin films on Si

Figure 5

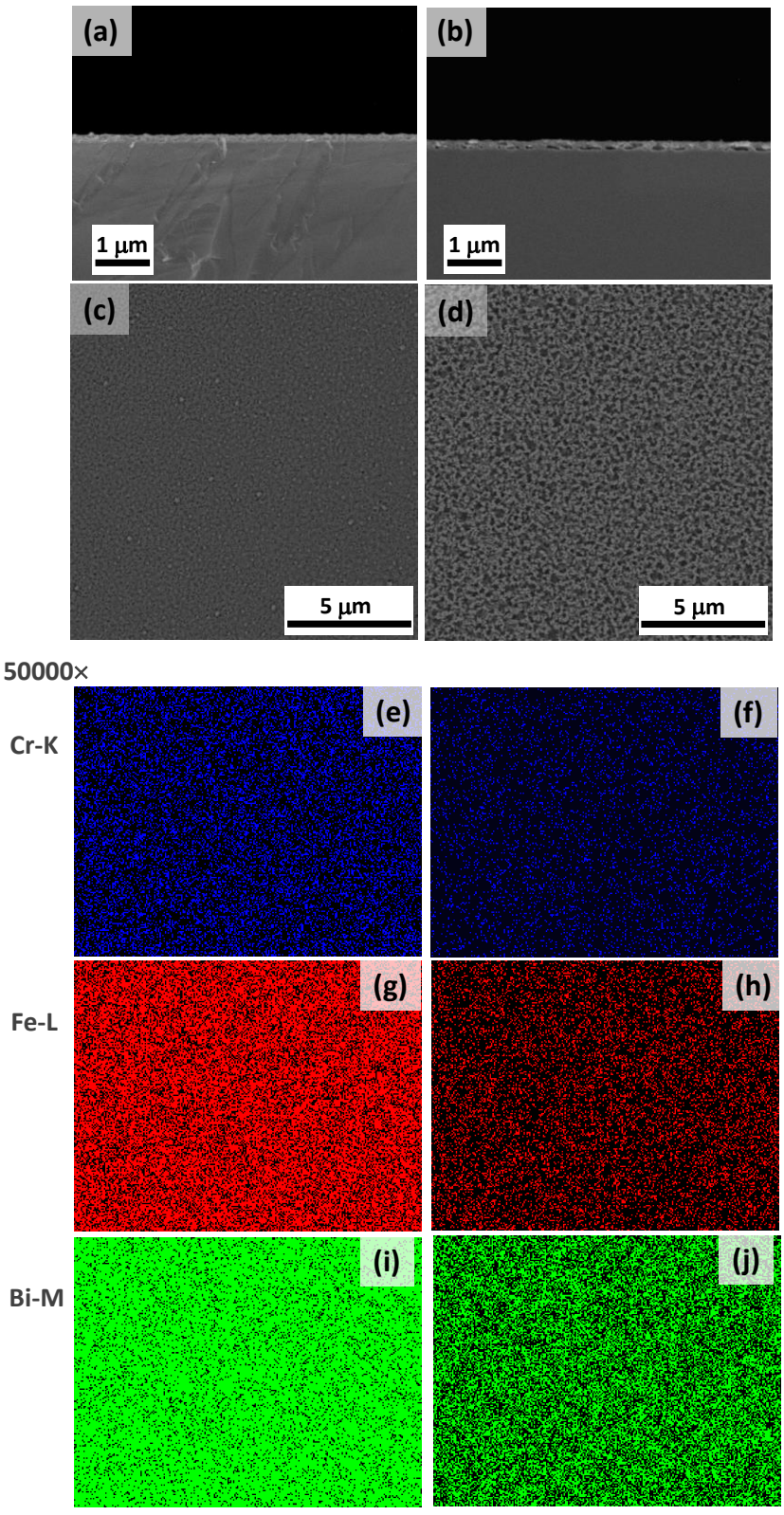

Figure 6

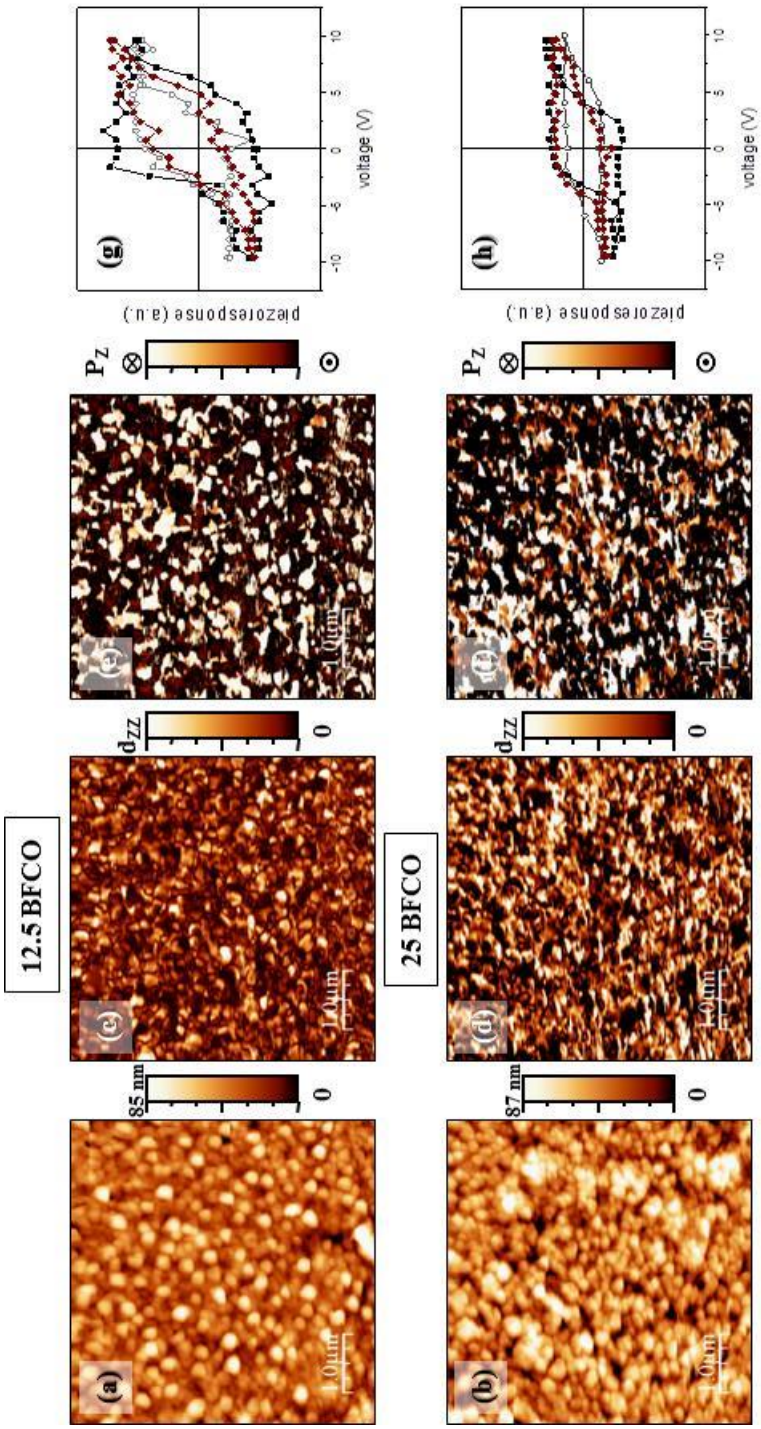
12.5 BFCO
25 BFCO
(a)
(b)
(c)
(d)
(e)
(f)
(g)
(h)
85 nm
87 nm
0
d_{ZZ}
P_Z
piezoresponse (a.u.)
voltage (V)
1.0 μm

Figure 7

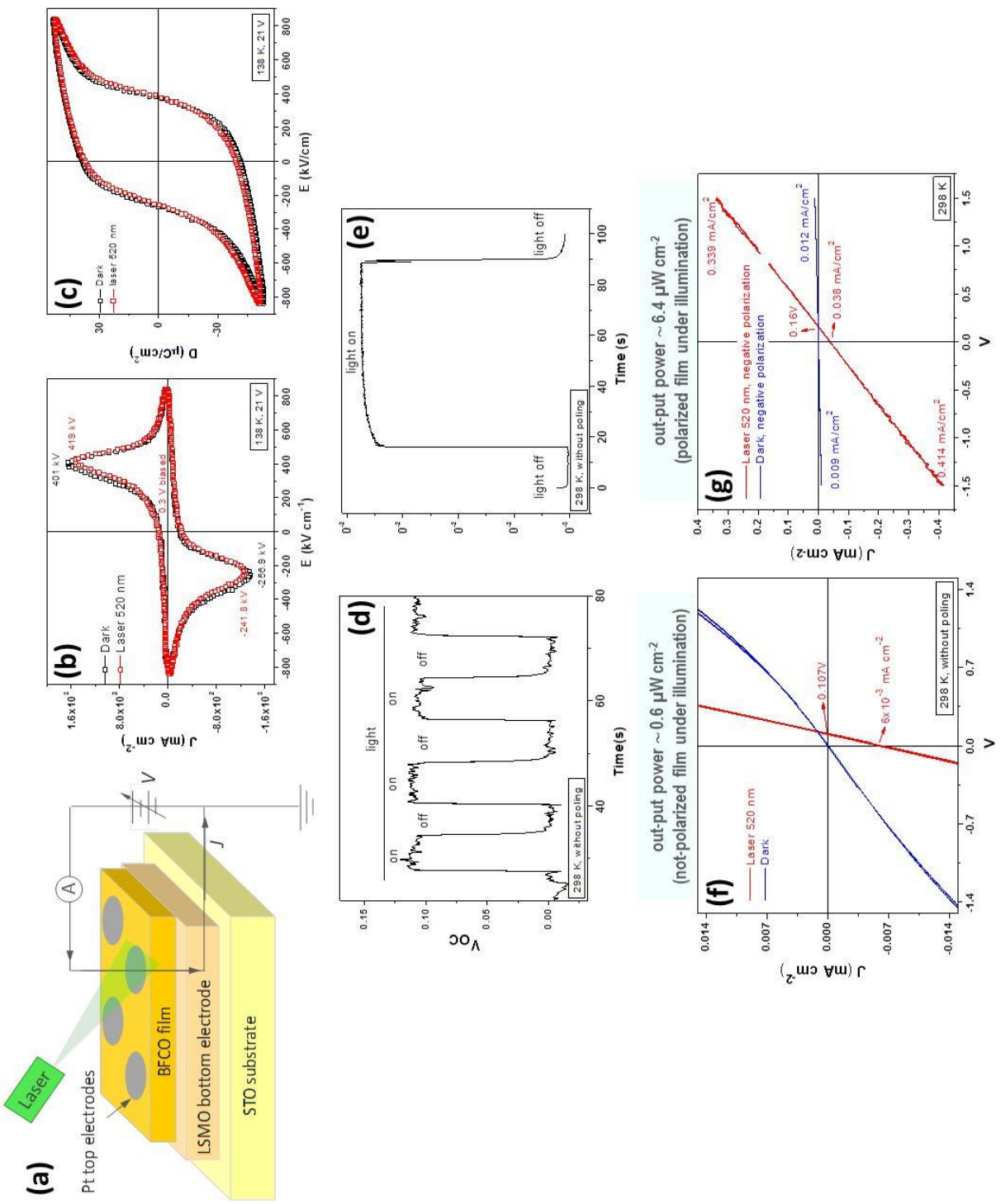
(a)
Laser
Pt top electrodes
BFCO film
LSMO bottom electrode
STO substrate
A
V
J
(b)
Dark
Laser 520 nm
401 kV
419 kV
0.3 V biased
-241.8 kV
-256.9 kV
138 K, 21 V
J (mA cm-2)
E (kV cm-1)
(c)
Dark
laser 520 nm
138 K, 21 V
D (μC/cm2)
E (kV/cm)
(d)
light
on
off
298 K, without poling
Voc
Time(s)
(e)
light on
light off
298 K, without poling
Time (s)
(f)
out-put power ~ 0.6 μW cm-2
(not-polarized film under illumination)
Laser 520 nm
Dark
0.107V
6x10-3 mA cm-2
298 K, without poling
J (mA cm-2)
V
(g)
out-put power ~ 6.4 μW cm-2
(polarized film under illumination)
Laser 520 nm, negative polarization
Dark, negative polarization
0.339 mA/cm2
0.16V
0.012 mA/cm2
0.038 mA/cm2
0.009 mA/cm2
0.414 mA/cm2
298 K
J (mA cm-2)
V

Figure 8